Load Distribution on a Close-Coupled Wing Canard at Transonic Speeds

Blair B. Gloss* and Karen E. Washburn†
NASA Langley Research Center, Hampton, Va.

This paper reports on a wind-tunnel test where load distributions were obtained at transonic speeds on both the canard and wing surfaces of a close-coupled wing-canard configuration. The investigation included detailed component and configuration arrangement studies to provide insight into the various aerodynamic interference effects for the leading-edge vortex flow conditions encountered. Data indicate that increasing the Mach number from 0.70 to 0.95 caused the wing leading-edge vortex to burst over the wing when the wing was in the presence of the high canard. For some of the outboard span locations, the leading-edge vortex reattachment streamline intersects the wing trailing edge inboard of these span locations; thus, the Kutta condition was not satisfied. In general, the effect of adding a canard was to reduce the lift inboard and somewhat increase the lift outboard similar to the trends that would have been expected had the flow been attached.

Nomenclature

b	= model semispan, cm
b^*	= exposed wing semispan, cm
c	= local chord, cm
c_{avg}	= average chord length, cm
$\bar{c}$	= mean geometric chord, cm
c_r	= chord length at fuselage-wing juncture
c_n	= section normal force coefficient
$C_{L,W}$	= lift on aft body and wing (Ref. 4)
C_p	= pressure coefficient
$C_p{}^*$	= sonic pressure coefficient
ΔC_p	= C_p upper surface $- C_p$ lower surface
$(\Delta C_p)_c$	= ΔC_p canard-on $- \Delta C_p$ canard-off
M	= Mach number
S	= wing reference area (wing extended to model centerline), cm^2
x	= longitudinal distance, cm
y'	= lateral distance, measured from wing-fuselage intersection, cm
z	= height above midchord plane of model, cm
α	= angle of attack, deg
Λ	= leading-edge sweep, deg
Λ_{isobar}	= isobar sweep, deg
η	= y'/b^*
γ	= ratio of specific heats

Introduction

PAST investigations[1-13] have indicated that the proper use of canard surfaces on maneuvering aircraft can offer several attractive features such as potentially higher trimmed-lift capability, improved pitching moment characteristics, and reduced trimmed drag. In addition, the geometric characteristics of close-coupled canard configurations offer a potential for improved longitudinal progression of cross-sectional area which could result in reduced wave drag at low supersonic speeds and placement of the horizontal control surfaces out of the high wing downwash and jet exhaust. Flow visualization studies[13] and analytical studies[14,15] have indicated that the favorable interference of the canard on the wing's lift produces a complex flowfield on the wing surface. Although there have been several papers published discussing the total forces and moments produced by close-coupled canard-wing configurations, very little data are available on the load distribution on canard and wing surfaces for close-coupled canard-wing configurations.

This paper reports on a wind-tunnel investigation where load distributions were measured at transonic speeds on both the canard and wing surfaces of a close-coupled wing-canard configuration. The investigation included detailed component and configuration arrangement studies to provide insight into the various aerodynamic interference effects. In addition to the detailed pressure measurements, the pressures have been integrated to illustrate the effects of Mach number, canard location, and canard-wing interference effects on various aerodynamic parameters. The present investigation was conducted in the Langley 8-ft transonic pressure tunnel. The tests were made at Mach numbers from 0.70 to 1.20 for Reynolds numbers, based on mean geometric chord, of 1.35×10^6 to 1.61×10^6 at angles of attack from approximately 0 to 20 deg and 0 deg sideslip.

Description of Model

A drawing of the model used in the wind-tunnel test (discussed in this paper) is presented in Fig. 1. This model was designed so that various wing and canard planforms could be attached to the common fuselage and the positional relationship of the lifting surfaces (canards and wings) could also be varied. The wings and canards were instrumented with several pressure orifices; the upper surface orifices were

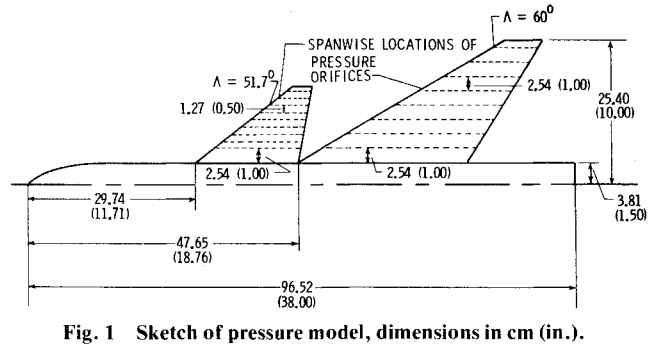

Fig. 1 Sketch of pressure model, dimensions in cm (in.).

Presented as Paper 77-1132 at the AIAA 4th Atmospheric Flight Mechanics Conference, Hollywood, Fla., Aug. 8-10, 1977; submitted Aug. 25, 1977; revision received Dec. 21, 1977.

Index categories: Aerodynamics; Transonic Flow.

*Aerospace Technologist.

† Aerospace Technologist. AIAA Student Member.

Table 1 Geometric characteristics

	Wing	Canard
b, cm	25.4	17.25
b^*, cm	21.6	13.4
Λ, deg	60	51.7
Airfoil section	circular arc	circular arc
S (wing area extended to plane of symmetry), cm^2	1032.2	...
Root chord (wing-body juncture), cm	29.8	17.92
Tip chord, cm	6.77	3.59
Maximum thickness, percent chord, at		
Root	6	6
Tip	4	4

Table 2 Configuration angle of attack

Configuration	α, deg $M=0.70$	$M=0.95$	$M=1.20$
High canard			
Canard-on	12.67	12.97	13.06
Canard-off	12.30	12.39	...
Mid-canard			
Canard-on	12.63	12.89	...
Canard-off	12.27	12.33	...
Low canard			
Canard-on	12.55	12.73	...
Canard-off	12.31	12.38	...

located on one lifting surface (wing or canard) and the lower surfaces orifices were located on the lifting surface on the other side of the model. However, both the instrumented canards and instrumented wings could not be tested simultaneously because of space restrictions in the model; thus, when both the canards and wings were on the model at the same time, either the wings or canards were uninstrumented. Table 1 presents the pertinent geometric parameters associated with this model.

The 60-deg swept untwisted wing had uncambered circular-arc airfoil sections and maximum thickness which varied linearly from 6% of the chord at the root (the root in this paper is the intersection of the fuselage and wing) to 4% of the chord at the tip.

The canard had a leading-edge sweep angle of 51.7 deg and an exposed area of 28.0% of the wing reference area S. The canard was tested in the chord plane of the wing ($z/\bar{c}=0.0$) and in positions 18.5% of the wing mean geometric chord above and below the wing chord plane ($z/\bar{c}=0.185$ and -0.185). To obtain the configuration with the canard located below the wing chord plane, the model with the canard in the high position was rolled 180 deg on the sting. The canard was untwisted and had uncambered circular-arc airfoil sections. The maximum thickness varied linearly from 6% of the chord at the root to 4% at the tip.

Results and Discussion

Although load distributions were obtained on both the canard and wing surfaces, this paper will focus on only the wing loads since the wing-canard interference effects are more pronounced on the wing. All of the data presented will be for a nominal angle of attack of approximately 12.7 deg; the exact angle of attack for each configuration discussed is shown in Table 2.

Aerodynamic Force Characteristics

Because of the sharp leading edge and relatively high sweep of the wing, a leading-edge vortex is generated on the wing. To illustrate the effect of the leading-edge vortex on the aerodynamic forces and to provide background information related to the pressure results, some of the force results

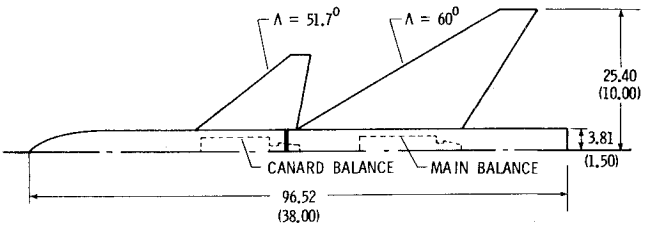

Fig. 2 Planform view of strain gage instrumented model.[4]

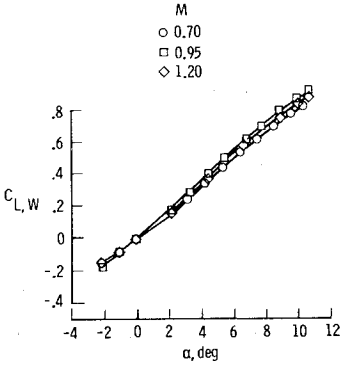

Fig. 3 Effect of Mach number on wing lift for the high-canard configuration.[4]

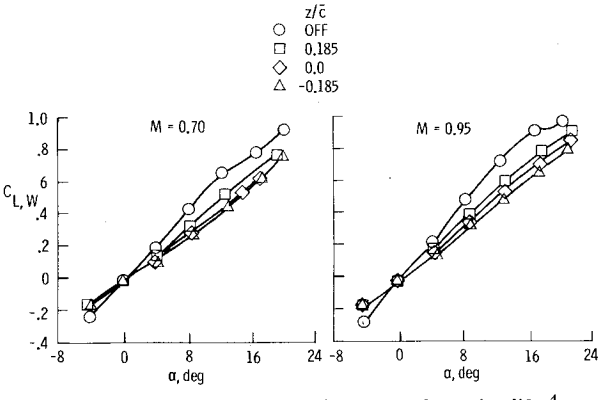

Fig. 4 Interference effect of the canard on wing lift.[4]

presented in Ref. 4, obtained on a geometrically identical model are presented herein. The wind-tunnel model discussed in Ref. 4 was instrumented with two strain gage balances, as shown in Fig. 2; one balance measured the load on the forebody and canards while the other balance measured the total load on the model. Figure 3 shows the effect of Mach number on wing lift, $C_{L,W}$ ($C_{L,W}$ is the difference between the lift on the main balance and the lift on the canard balance, see Fig. 2) for the high-canard configurations. Since this report will focus on only the pressure distribution of the wing, only the wing lift is reproduced from Ref. 4; for more complete information the reader is referred to Ref. 4. In this paper, the high canard is located at $z/\bar{c}=0.185$, the mid-canard at $z/\bar{c}=0.0$, and the low canard at $z/\bar{c}=-0.185$.

The data in Fig. 3 show that there are only small effects of Mach number on the total life, as would be expected from the relatively high sweep angles. The effect of canard location on wing lift is shown in Fig. 4. These data indicate that the canard downwash substantially reduces the wing lift over the angle-of-attack range shown. In general, the low canard reduces the lift on the wing the most and the high canard the least. It can be seen in Fig. 4 that for the $M=0.95$ case, the wing not in the presence of the canard appears to stall, the leading-edge vortex bursts over the wing at some angle of attack greater than 12 deg, while the wing in the presence of the canards show no sign of wing stall. To indicate some of the problems involved with predicting the total load versus

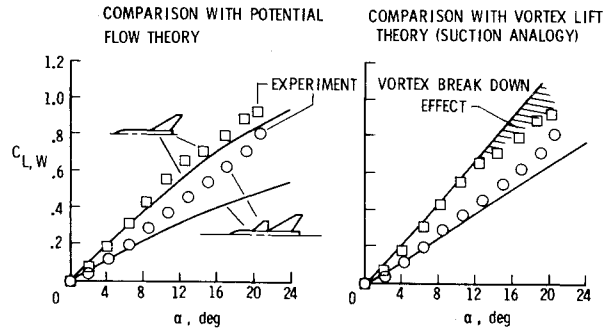

Fig. 5 Comparison of experimental and theoretical canard interference effect on wing lift, $M = 0.70$.[4]

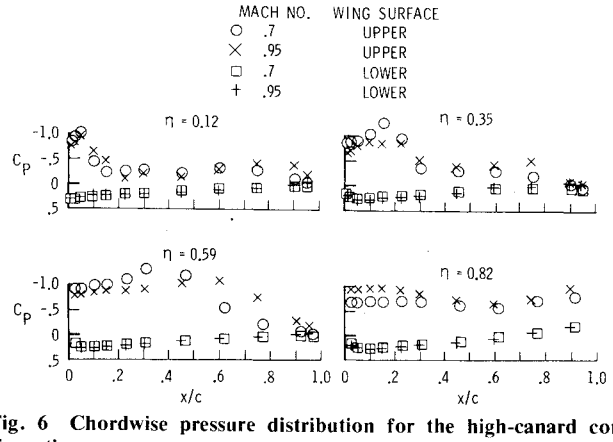

Fig. 6 Chordwise pressure distribution for the high-canard configuration.

angle of attack for a wing in the presence of a canard, Fig. 5 shows a comparison of experimental and theoretical wing lift. On the left, the data are compared with potential flow theory and on the right with vortex lift theory. Since the wing is swept 60 deg and produces a separation-induced leading-edge vortex, the underprediction of lift using potential flow theory should be expected for both the wing in the presence of the canard and the wing-alone configurations. It is of interest to note, however, that with the wing in the presence of the canard, the increase in wing lift over potential flow theory is much greater and at high angles of attack nearly offsets the downwash effect from the canard. The vortex lift theory agrees well with experiment for the wing-alone case up to an angle of attack of approximately 13 deg, where the leading-edge vortex appears to burst in the vicinity of the wing. However, for the wing in the presence of the canard, no breakdown effect is evident and the lift exceeds that predicted by the vortex lift theory. It is assumed that the additional vortex lift implied by the comparison may be associated with a stablizing effect on and possibly an augmentation of the wing leading-edge vortex by the canard flowfield.

Effect of Mach Number on Wing Loads in the Presence of a Canard

Mach numbers 0.70 and 0.95 chordwise pressure distribution data on the wing for the high-canard configuration are shown in Fig. 6. The chordwise pressure distribution for the 0.70 Mach number case indicates that there is a leading-edge vortex which washes back over the wing; however, the 0.95 Mach number case indicates a leading-edge vortex inboard, and there appears that there may be a vortex washing back over the wing, but these data are not conclusive. In the span region of $\eta = 0.82$, it is seen that the Kutta condition tends not to be satisfied for either Mach number. For a further understanding of the flowfield on the wing at these Mach numbers, Figs. 7 and 8 show isobars on the wing in the presence of the high canard and with the canard removed for $M = 0.70$ and 0.95.

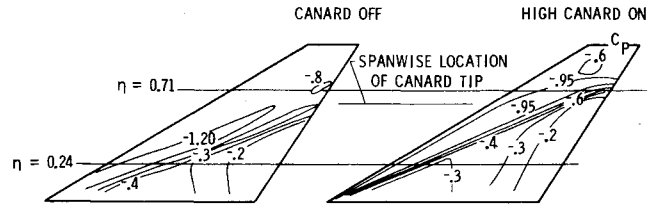

Fig. 7 Lines of constant pressure for canard-off and high-canard-on configurations for a Mach number of 0.70.

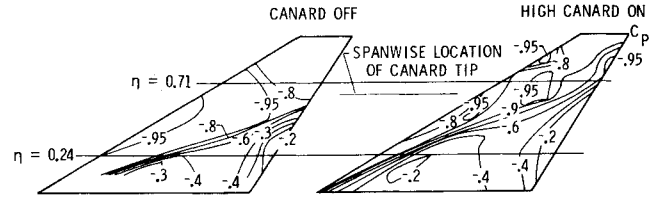

Fig. 8 Lines of constant pressure for canard-off and high-canard-on configurations for a Mach number of 0.95.

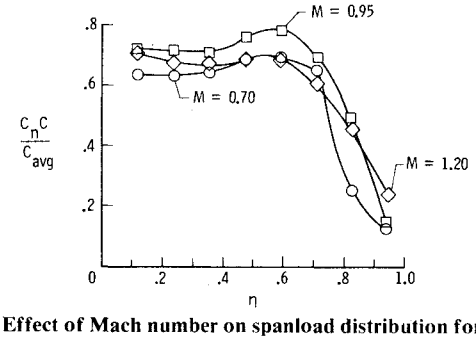

Fig. 9 Effect of Mach number on spanload distribution for the high-canard configuration.

For isobars swept 66 deg, which is a nominal sweep angle for the canard on configuration at Mach numbers of 0.70 and 0.95 (Figs. 7 and 8), $C_p{}^*$ is -1.29 and -0.66, respectively. Equation (1) defines $C_p{}^*$:

$$C_p{}^* = \frac{2}{\gamma M^2}\left\{\left[\frac{2}{\gamma+1}\left(1+\frac{\gamma-1}{2}M^2(\cos\Lambda_{\text{isobar}})^2\right)\right]^{\gamma/\gamma-1}-1\right\} \tag{1}$$

The flow appears to be everywhere subcritical for the $M = 0.70$ case. For $M = 0.95$, there is a shock wave which has generally the same sweep as the isobars in the leading-edge section of the wing out to a span station of $\eta \approx 0.35$; since further outboard of $\eta \approx 0.35$ the isobars tend to unsweep, the flow on this region of the wing is probably all supersonic. For both Mach numbers the leading-edge vortex is delineated by the isobars in Figs. 7 and 8.

The data in Fig. 6 indicate that the Kutta condition is not satisfied at the $\eta = 0.82$ span station. For the $M = 0.70$ case this is probably due to the vortex-induced reattachment line being located inboard of this span station, Fig. 7; and for $M = 0.95$, the apparent unsatisfied Kutta condition may be due to the supersonic flow on the wing at this station.

For $M = 0.95$, the $C_p = -0.95$ isobar closes on itself in the vicinity of $\eta = 0.71$ (Fig. 8). It is suggested that the vortex bursts at this location, causing a rapid growth of the vortex core, and the vortex burst bubble is defined by the $C_p = -0.95$ isobar. Even though the vortex has burst, it is felt that there is still circulation around it, and the far-field flow, above the wing, is still organized, since the total lift on the wing for the $M = 0.95$ case shows little indication of loss of lift due to vortex bursting (Fig. 3).

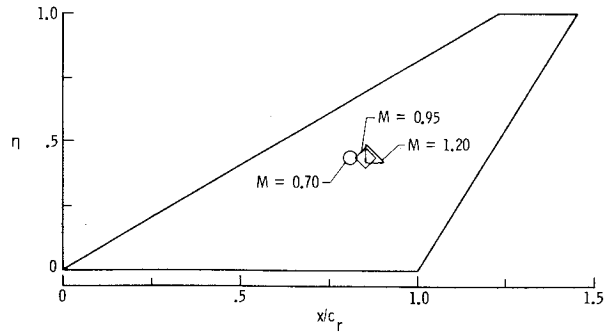

Fig. 10 Effect of Mach number on center-of-pressure location for the high-canard configuration.

The effect of Mach number on the span load distribution is shown in Fig. 9 for the wing in the presence of the high canard. The span loads seem to correlate well with the total loads shown in Fig. 3. In the description of the model, it was pointed out that the wing was uncambered and untwisted with a sharp leading edge; thus, optimum span loads, as regards induced drag, should not be expected. Integrating these loads, in Fig. 9, yields the center-of-pressure locations shown in Fig. 10 for the wing in the presence of the high-canard at three Mach numbers. As might be expected, there is a rearward movement of center of pressure with Mach number; this rearward movement is approximately 5% of the mean geometric chord of the wing. It is interesting to note that, although there are substantial differences in the character of flow in going from a Mach number of 0.70 to 0.95 (Figs. 6-8), there is essentially no spanwise movement of the center of pressure.

Effect of Canard Location on Wing Loads

In order to help explain some of the pressure distribution results that will be presented in this section, a brief discussion of some of the flow visualization results of Ref. 13 is in order. These flow pictures indicate that for the high- and mid-canard positions, the canard wake is well above the wing upper surface for an angle of attack of 12.7 deg; thus, although induced effects can occur, the canard wake does not physically interfere with the wing for these two configurations at this angle of attack. However, the flow pictures of Ref. 13 indicate that the wing is in the wake of the low canard much of the time; therefore, since the wing is in this low-energy wake, it is expected that the wing in the presence of a low canard will lose substantial lift.

Chordwise pressure distributions at two spanwise stations, $\eta = 0.24$ and 0.71, are shown in Figs. 11 and 12 for the wing in the presence of the high canard and wing alone at two Mach numbers, 0.70 and 0.95. For both Mach numbers, the effect of the canard downwash at the inboard station, $\eta = 0.24$, on both the upper and lower surfaces is, of course, to reduce the effective angle of attack of this station. In addition to apparently weakening the strength of the leading-edge vortex of the wing at this inboard station, the interference of the canard on the wing moves the leading-edge vortex forward. At the outboard station, $\eta = 0.71$, there is evidence of the leading-edge vortex passing over a rather aft chordwise location for both Mach numbers for the canard-on configuration; while, for the canard-off configuration, there is little evidence of a vortex at the $\eta = 0.71$ span station. The Kutta condition is not satisfied at the $\eta = 0.71$ station for the canard-off configuration; Figs. 11 and 12 seem to indicate that this is so because this particular section is stalled. The isobar plots in Figs. 7 and 8 show a little more graphically that the effect of the canard interference is to move the leading-edge vortex forward and improve the flow on the outboard sections of the wing. Thus, even with leading-edge vortex flow, the net effect of the canard is to decrease the load inboard and increase the load outboard as would be expected with attached flow.

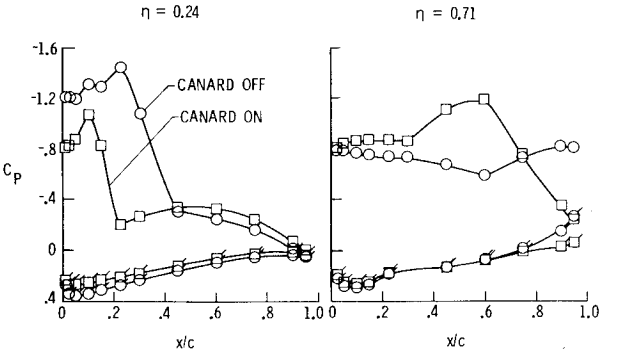

Fig. 11 Wing chordwise pressure distribution for the high-canard configuration at a Mach number of 0.70; flagged symbols are lower surface.

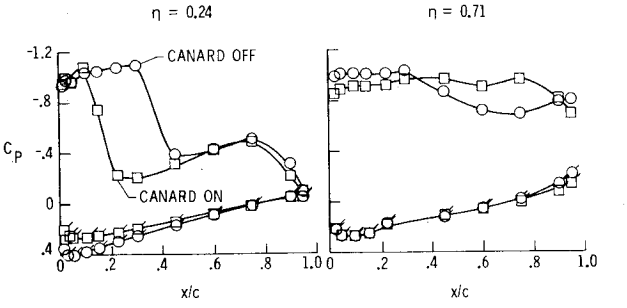

Fig. 12 Wing chordwise pressure distribution for the high-canard configuration at a Mach number of 0.95; flagged symbols are lower surface.

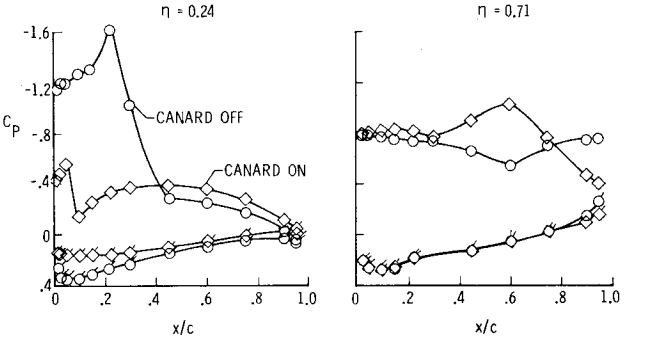

Fig. 13 Wing chordwise pressure distribution for the mid-canard configuration at a Mach number of 0.70; flagged symbols are lower surfaces.

Since, for the mid-canard configuration, the canard wake is located physically closer to the wing than for the high-canard configuration, stronger effects of canard downwash on the wing should be expected for, at least, the inboard wing stations. Figures 13 and 14 show that this speculation is correct; the pressure distributions at span station $\eta = 0.24$, show a much stronger effect of canard downwash on the wing pressure distribution for the mid-canard than for the high canard. In fact, as mentioned earlier, for the high-canard configuration, there appeared to be a shock wave located at the $\eta = 0.24$ span station at $M = 0.95$, but the downwash of the canard on the wing appears to have suppressed the shock wave at $M = 0.95$, for the mid-canard configuration [$C_p{}^*(@\,\Lambda_{\text{isobar}} = 66 \text{ deg}) = -0.67$]. As with the high-canard configuration, the interference effects of the canard on the wing appear to enhance the vortex at the outboard station, $\eta = 0.71$. Again, as discussed earlier, the vortex reattachment streamline intersects the wing trailing edge inboard of the $\eta = 0.71$ station and, thus, the Kutta condition is not satisfied.

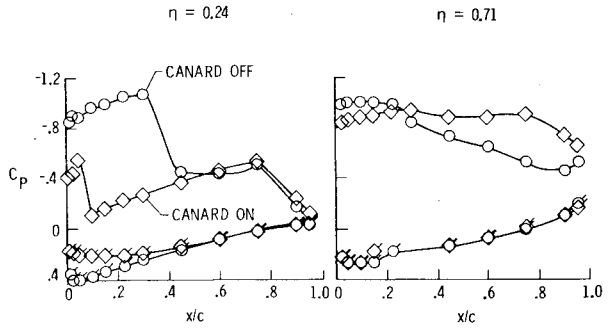

Fig. 14 Wing chordwise pressure distribution for the mid-canard configuration at a Mach number of 0.95; flagged symbols are lower surfaces.

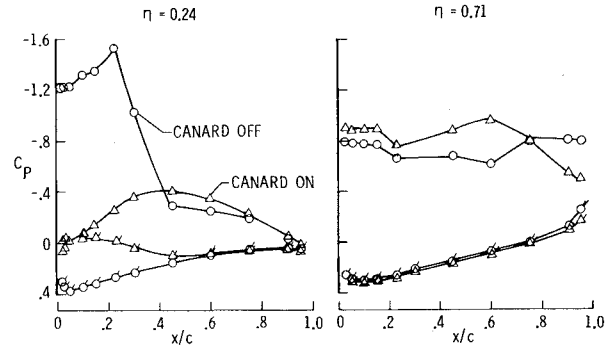

Fig. 15 Wing chordwise pressure distribution for the low-canard configuration at a Mach number of 0.70; flagged symbols are lower surfaces.

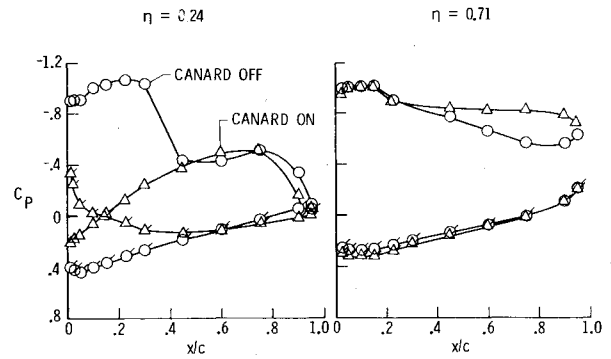

Fig. 16 Wing chordwise pressure distribution for the low-canard configuration at a Mach number of 0.95; flagged symbols are lower surfaces.

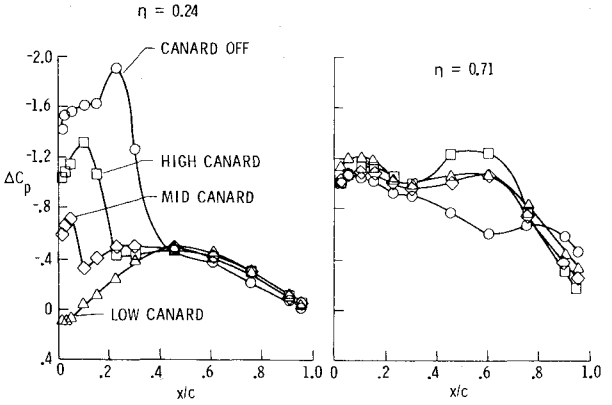

Fig. 17 Effect of canard location on wing lifting pressure at a Mach number of 0.70.

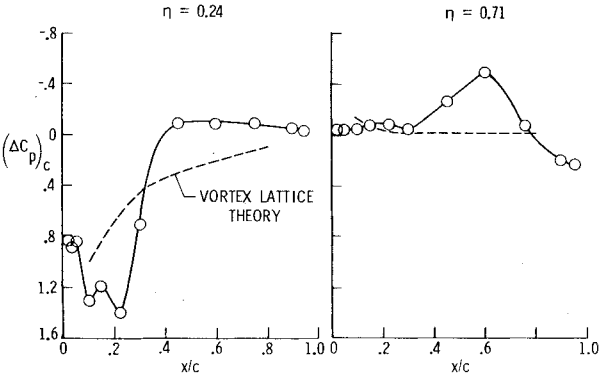

Fig. 18 Effect of canard on wing lifting pressure for the mid-canard at a Mach number of 0.70.

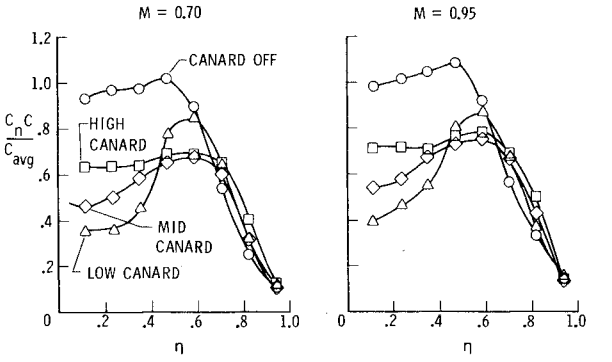

Fig. 19 Effect of canard location on wing spanload distribution.

The effect of the interference of the low canard on the inboard station, $\eta = 0.24$, completely changes the character of the pressure distribution from what had occurred for the high- and mid-canard configurations, Figs. 15 and 16. From the flow visualization pictures presented in Ref. 13, this rather drastic change in pressure distribution appears to be due to the wake of the canard physically interacting with the wing. The outboard station appears to be very similar to the other two configurations.

A summary of the effect of canard position on wing lifting pressure for a Mach number of 0.70 is shown in Fig. 17. As should be expected from the earlier discussion, it is seen that for the inboard sections, the canard affects the front portion of the wing, while outboard, the largest effects of canard are on the aft portion of the wing. Using these results in Fig. 17, Fig. 18 presents a plot comparing attached flow theory with experiment; plotted is the difference between lifting pressure for canard-on and canard-off. Of course, attached flow theory should not be expected to agree well with the experiment since the flow is separated for this model. However, in the absence of any better theory, the attached flow theory is presented. The theory, of course, thus misses the vortex on both the inboard and outboard sections. The data in Fig. 18 do show the magnitude of the error incurred when potential flow theory is used to compute the canard interference effect on the wing when the wing has a leading-edge vortex and emphasizes the need for loads prediction methods that accurately account for vortex flows.

The effect of canard location at Mach numbers of 0.70 and 0.95 on the span load distribution is presented in Fig. 19. In general, it is seen that on the inboard section of the wing, the low-canard configuration loses the most lift and the high canard the least. While on the outboard section of the wing, all three canard configurations produce more lift than the canard-off configuration. This is due to the enhanced leading-edge vortex passing over this section of the wing for the canard configurations.

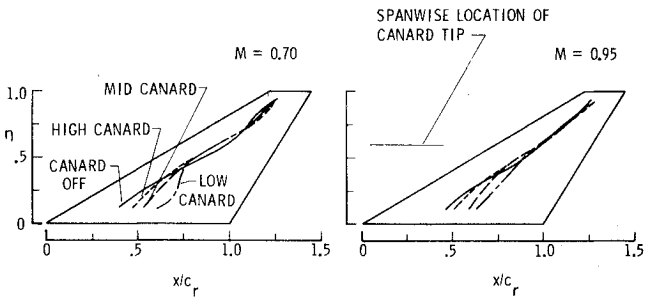

Fig. 20 Effect of canard location on sectional center-of-pressure location.

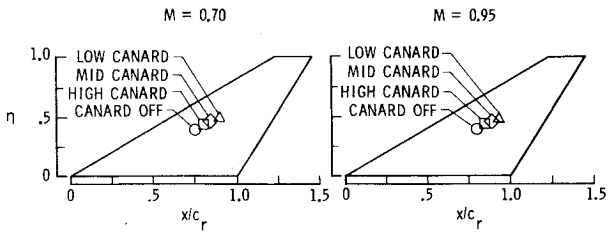

Fig. 21 Effect of canard location on center-of-pressure location.

Figure 20 shows the center-of-pressure location for each chordwise station plotted for the canard-off configuration and the three canard configurations. There is little effect of the canard on the outboard sectional center of pressures. However, for the wing inboard stations, moving the canard from the high position to low moves the center of pressure rearward for both Mach numbers shown. Further integration of the span load distributions yields the total center of pressure, as is shown in Fig. 21 for Mach numbers 0.70 and 0.95. The effect of adding a canard to the wing load is to move the center of pressure rearward and outward.

Concluding Remarks

The transonic load distribution has been experimentally determined for a wing ($\Lambda = 60$ deg) which had leading-edge vortex flow and which was in the presence of a canard located above, in, and below the wing chord plane. Although there are substantial differences in the character of the flowfield in going from a Mach number of 0.70 to 0.95, there are only small changes in the center of the pressure location and in the wing lift.

The effect of canard downwash, for the canard located above and in the wing chord plane, is to decrease the effective angle of attack of those wing stations immediately behind the canard, and this sustantially weakens the wing leading-edge vortex. This vortex weakening delays the leading-edge vortex burstings. As might be expected, the canard downwash effects are greater for the canard located in the wing chord plane, since it is physically closer to the wing. The downwash effect of the canard located below the wing was to completely change the character of the wing flowfield immediately behind the canard; it is suggested that the wing is in the canard wake at the angle of attack presented.

References

[1] McKinney, L. W. and Dollyhigh, S. M., "Some Trim Drag Considerations for Maneuvering Aircraft," *Journal of Aircraft*, Vol. 8, Aug. 1971, pp. 623-629.

[2] Dollyhigh, S. M., "Static Longitudinal Aerodynamic Characteristics of Close-Coupled Wing-Canard Configurations at Mach Numbers From 1.60 to 2.86," NASA TN D-6597, 1971.

[3] Gloss, B. B. and McKinney, L. W., "Canard-Wing Lift Interference Related to Maneuvering Aircraft at Subsonic Speeds," NASA TM X-2897, 1973.

[4] Gloss, B. B., "Effect of Canard Height and Size on Canard-Wing Interference and Aerodynamic Center Shift Related to Maneuvering Aircraft at Transonic Speeds," NASA TN D-7505, 1974.

[5] Gloss, B. B., "The Effect of Canard Leading-Edge Sweep and Dihedral Angle on the Longitudinal and Lateral Aerodynamic Characteristics of a Close-Coupled Canard Wing Configuration," NASA TN D-7814, 1974.

[6] Gloss, B. B., "Effect of Wing Planform and Canard Location and Geometry on the Longitudinal Aerodynamic Characteristics of a Close-Coupled Canard Wing Model at Subsonic Speeds," NASA TN D-7910, 1975.

[7] Behrbohm, H., "Basic Low Speed Aerodynamics of the Short-Coupled Canard Configuration of Small Aspect Ratio," Saab Aircraft Co., Linkoping, Sweden, SAAB TN-60, July 1965.

[8] Lacey, D. W. and Chorney, S. J., "Subsonic Aerodynamic Characteristics of Close-Coupled Canards with Varying Area and Position Relative to a 50° Swept Wing," Naval Ship Research and Development Center, TN AL-199, March 1971.

[9] Ottensoser, J., "Wind Tunnel Data on the Transonic Aerodynamic Characteristics of Close-Coupled Canards With Varying Planform Position and Deflection Relative to a 50° Swept Wing," Naval Ship Research and Development Center, TR AL-88, May 1972.

[10] Krouse, J. R., "Effects of Canard Planform on the Subsonic Aerodynamic Characteristics of a 25° and a 50° Swept Wing Research Aircraft Model," Naval Ship Research and Development Center, Evaluation Rept. AL-91, Aug. 1972.

[11] Lacey, D. W., "Transonic Characteristics of Close-Coupled Canard and Horizontal Tail Installed on a 50 Degree Sweep Research Aircraft Model," Naval Ship Research and Development Center, Evaluation Rept. AL-8, Aug. 1972.

[12] Gloss, B. B., Henderson, W. P., and Huffman, J. K., "Effect of Canard Position and Wing Leading-Edge Flap Deflection on Wing Buffet at Transonic Speeds," NAS TM X-72681, 1975.

[13] Miner, D. D. and Gloss, B. B., "Flow Visualization Study of Close-Coupled Canard-Wing and Strake-Wing Configuration," NASA TM X-72668, 1975.

[14] Lamar, J. E. and Gloss, B. B., "Subsonic Aerodynamic Characteristics of Interacting Surfaces With Separated Flow Around Sharp Edges Predicted by a Vortex-Lattice Method," NASA TN D-7921, 1975.

[15] Lamar, J. E., "Some Recent Applications of the Suction Analogy to Vortex-Lift Estimates," NASA TM X-72785, 1976.